Back to Session Subjects

DESIGN AND TESTING OF THE NASA/ARMY/MIT ACTIVE TWIST ROTOR PROTOTYPE BLADE

Carlos E. S. Cesnik, SangJoon Shin

Active Materials and Structures Laboratory, Department of Aeronautics and Astronautics, Massachusetts Institute of Technology, Cambridge, MA 02139, USA

Matthew L. Wilbur, and W. Keats Wilkie

Army Research Laboratory, NASA Langley Research Center, Hampton, VA 23681, USA.

Abstract

The development of an active twist rotor (ATR) blade is investigated analytically and experimentally in this paper. The ATR system is intended for vibration and potentially noise reductions in helicopters through individual blade control. An aeroelastic model is developed to identify frequency response characteristics of the ATR blade with integral, generally anisotropic, strain actuators embedded in its composite construction. An ATR blade was also designed and manufactured to experimentally study the vibration reduction capabilities of such systems. Several bench tests and wind tunnel hover tests were conducted at MIT and NASA Langley, respectively. Those results are presented and discussed here. Using the developed active blade model, numerical results are compared to non-rotating and rotating experimental data. The proposed model captures the physical trends and sensitivities to selected test parameters. Correlation on the bench is excellent, supporting the new active structural dynamics model of ATR blades. The numerical results of the blade torsional loads in hover are qualitatively excellent, and average error of 20% in magnitude is observed. Overall, the active rotor blade model is in very good agreement with the experiments and can be used to analyze and design future active blade systems.

1 Introduction

The technology of smart structures provides a new degree of design flexibility for individual blade control (IBC) of advanced composite helicopter rotor blades.[1-2] The key to the technology is the ability to allow the structure to sense and react in a desired fashion, with potential improvements in rotor blade performance, especially in the areas of structural vibration, acoustic signature, and aeroelastic stability.

The broad class of actuation approaches for helicopter IBC can be basically subdivided in two groups: actuated control surfaces at discrete locations along the blade,[3-9] and direct deformation (usually twist) of the blade structure.[10-14] The present work falls on the latter.

Recent analytical and experimental investigations have indicated that the active fiber composites (AFC) embedded in composite rotor blade structures should be capable of meeting the performance requirements necessary for a useful individual blade control system.[12-14] The AFC actuator utilizes interdigitated electrode poling and piezoelectric fiber embedded in an epoxy matrix[15]. This combination results in a high performance piezoelectric actuator laminate with strength and conformability characteristics much greater than that of a conventional monolithic piezoceramic. Among the efforts in this area of direct deformation of the blade using AFC actuators is the collaborative program between Boeing Co. and MIT (sponsored by DARPA). This program has been addressing the different manufacturing issues of an integrally twisted blade using the AFC actuators. A single Mach-scaled model blade was constructed and hover tests were conducted, showing encouraging results.[13] Future design and manufacturing of a three-bladed rotor system is expected to happen for eventual Mach-scaled wind tunnel tests in air (where specific demonstrations of full-scale blade stresses will be possible).

In a complementary manner, a research program between NASA Langley/Army Research Laboratory and MIT has been established to investigate the specific issues related to the modeling and design of Active Twist Rotor (ATR) systems, evaluate their effectiveness for IBC in forward flight, and the impact on vibration and noise reduction, as well as potential cyclic control of future active systems. As part of the ATR study, extensive wind tunnel test will support the proposed concept and will provide a first-of-a-kind experimental data for validation of the concept and the developed active blade-modeling framework. The tests are conducted using a 2.74-m diameter 4-bladed fully-articulated aeroelastically scaled wind tunnel model designed for testing in the heavy gas environment of the NASA Langley Transonic Dynamics Tunnel (TDT). The Aeroelastic Rotor Experimental System (ARES), shown in the TDT in

Fig. 1, is used to test the ATR model. The TDT utilizes a heavy gas test medium with a speed of sound approximately one half that of sea level standard air. This, as well as the TDT's variable density test capability, permits full scale rotor tip Mach numbers, Froude numbers, and Lock numbers to be matched simultaneously at model scale. In particular, the reduced speed of sound in the heavy gas medium allows full-scale tip Mach numbers to be matched at lower rotational speeds and lower blade stresses.

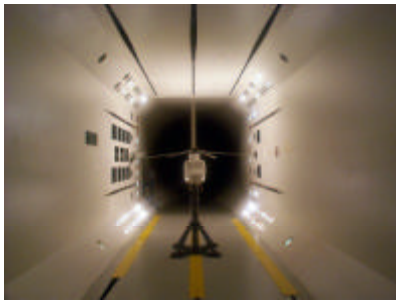

Figure 1. The ARES testbed in the TDT with the ATR prototype blade installed.

This paper discuss the development of the ATR prototype blade: the framework developed for analyzing such blades, its design, manufacturing, and tests, both on the bench and in hover.

The general framework developed to analyze and design active composite blades is presented first. It models the blade as a multi-cell composite beam with embedded integral anisotropic actuators. This was the first attempt in the literature towards an asymptotical analysis of active multi-cell beams.[18] The asymptotical analysis takes the electromechanical three-dimensional problem and reduces it into a linear analysis over the cross section and a nonlinear analysis of the resulting beam reference line. The effects of the active material embedded in the structure are carried out throughout all the steps of the analysis. Validation of the developed model was conducted by correlating with other theoretical models and experimental data obtained from small-scaled active blades.[18]

Using the developed analysis and CAMRAD II estimates of critical forward flight loads, the design of the ATR blade is carried out based on an actuation authority requirement and considering the general static and dynamic characteristics of a generic research blade. A prototype blade was manufactured at MIT, and the principal steps are presented in this paper.

Bench test and preliminary hover test were conducted on the ATR prototype blade. For the hover test, the ATR prototype blade was installed at the rotor system hub along with three other (dummy) passive blades. The tests validate the design and manufacturing procedures, and verify the performance and dynamic characteristics of the prototype article. Actuation authority and vibration behavior in non-rotating condition and dynamic characteristics of the ATR blade and the overall rotor system in rotating conditions are discussed at the end. Correlation of the experimental data with the prediction of the developed theory used in the design of the blade is also presented. This supports the validation of the numerical model that is being built to study optimal twist actuation schemes for future individual blade control.

2 Theoretical Model

For analyzing helicopter blades with embedded strain actuators, a framework is needed such that the effects of the active material embedded in the structure are carried out throughout all the steps of the analysis. A new analysis formulation was created for active rotor blade modeling that is able to model realistic blade cross section like the one needed for the ATR concept. As described below, an asymptotical analysis takes the electromechanical three-dimensional problem and reduces it into a set of two analyses: a linear analysis over the cross section and a nonlinear analysis of the resulting beam reference line.

2.1 Cross-Section Analysis

The new asymptotical formulation to analyze multi-cell composite beams incorporating embedded piezoelectric plies distributed throughout the blade was developed and presented in detail in Ref. 18. While restricted to thin-walled beams, it yields closed form solutions of the displacement field (which is derived and *not* assumed), and stiffness and actuation constants. The availability of correct closed form expressions is essential to determine design paradigms on this new type of blade, mainly concerning to the tradeoffs between torsional stiffness and twist actuation. These stiffness and actuation constants will then be used in a beam finite element discretization of the blade reference line.

Even though the details of this formulation can be found in Ref. 18, the main results are reproduced below for completeness. With an assumed linear piezoelectric constitute relation and starting from a shell strain energy, the 2-D original electroelastic shell formulation is condensed to a 1-D beam problem. The displacement field is found to be of the form:

$$
\begin{aligned}
v_1 &= u_1(x) - y(s)u_2'(x) - z(s)u_3'(x) + \\
&\quad + G(s)f'(x) + g_1(s)u_1'(x) + \\
&\quad + g_2(s)u_2''(x) + g_3(s)u_3''(x) + v_1^{(a)}(s) \\
v_2 &= u_2(x)\frac{dy}{ds} + u_3(x)\frac{dz}{ds} + f(x)r_n \\
v_3 &= u_2(x)\frac{dz}{ds} - u_3(x)\frac{dy}{ds} - f(x)r_n
\end{aligned}
\tag{1}
$$

where the superscript *(a)* indicates that the component is function of the applied electric field (in the case of thin-walled cross sections, the actuation only influences the out-of-plane component of the displacement field). The functions $G(s)$ and $g_i(s)$ are the warping functions associated with torsion, extension, and two bending measures. Associated with this displacement field, the beam constitutive relation relating beam generalized forces (axial force, twist, and two bending moments, respectively) with beam generalized strains (axial strain, twist curvature, and two bending curvatures) and corresponding generalized actuation forces (function of the geometry, material distribution, and applied electric field) is obtained in the following form:

$$
\begin{Bmatrix} F_1 \\ M_1 \\ M_2 \\ M_3 \end{Bmatrix} = \begin{bmatrix} K_{11} & K_{12} & K_{13} & K_{14} \\ K_{12} & K_{22} & K_{23} & K_{24} \\ K_{13} & K_{23} & K_{33} & K_{34} \\ K_{14} & K_{24} & K_{34} & K_{44} \end{bmatrix} \begin{Bmatrix} g_{11} \\ k_1 \\ k_2 \\ k_3 \end{Bmatrix} - \begin{Bmatrix} F_1^{(a)} \\ M_1^{(a)} \\ M_2^{(a)} \\ M_3^{(a)} \end{Bmatrix} \tag{2}
$$

where $[K]$ is the stiffness matrix function of geometry and material distribution at the rotor cross section. From this formulation, all K_{ij} and the generalized actuation forces are given by closed form expressions.[18]

2.2 1-D Beam and Aerodynamics Analysis

The geometrically exact beam equations follow from the asymptotical analysis and include the distributed actuation. As direct extension of Ref. 19, the original nonlinear formulation allows for small strain and finite rotations, and is cast in a mixed variational intrinsic form. The embedded actuation effects come in the new constitutive relation that modifies the 1-D finite element formulation. Its implementation was performed on the aeroelastic hover solution described in Ref. 20, and details of that can be found in Ref. 21. The solution of the 1-D beam analysis provides blade displacement and generalized stress fields due to external loading and piezoelectric actuation, which are of interest in the analysis of static and dynamic deformations and aeroelastic stability.

Based on a thin airfoil theory, the external aerodynamic loads acting on the rotor blade surface are formulated in rotating conditions (either in hover or forward flight). Since the aerodynamic model used in this formulation contains the induced velocity terms explicitly, it is necessary to solve them simultaneously. In this analysis, finite-state dynamic inflow equations based on Peters and He[19] is adopted. In its derivation, new state-variables are generated to describe the inflow velocity at discrete spanwise locations by dynamic equilibrium equations between inflow quantities and pressure imposed on the rotor blades. These equations usually involve the structural variables and their time derivatives, such as displacements and rotations and, therefore, they need to be solved concomitantly with the structural equilibrium equations.

2.3 Solution of the Aeroelastic System

The structural equilibrium equations from 1-D beam analysis can be grouped into structural (F_S) and aerodynamic terms (F_L) as follows:

$$
F_S(X, \dot{X}, V) - F_L(X, Y, \dot{X}) = 0 \tag{3}
$$

where X is the vector of structural variables, Y the inflow variables, and V is the vector of magnitudes of the electrical field distribution shape. Similarly, the inflow dynamics can be represented by separation into pressure (F_P) and inflow (F_I) components:

$$
-F_P(X, Y) + F_I(Y, \dot{Y}) = 0 \tag{4}
$$

The solution of interest for the coupled set of equations above can be derived based on small perturbation from steady-state equilibrium:

$$
\begin{Bmatrix} X \\ Y \end{Bmatrix} = \begin{Bmatrix} \overline{X} \\ \overline{Y} \end{Bmatrix} + \begin{Bmatrix} \breve{X}(t) \\ \breve{Y}(t) \end{Bmatrix} \tag{5}
$$

For the solution of steady-state equilibrium, one needs to solve a set of nonlinear equations of both Eqs. (3) and (4):

$$
\begin{cases} F_S(\overline{X}, 0, \overline{V}) - F_L(\overline{X}, \overline{Y}, 0) = 0 \\ -F_P(\overline{X}, \overline{Y}) + F_I(\overline{Y}, 0) = 0 \end{cases} \tag{6}
$$

The Jacobian matrix of the above set of nonlinear equations can be obtained analytically and is found to be very sparse. The steady-state equilibrium solution can be found very efficiently using Newton-Raphson method.

In order to investigate the dynamic response of the blade with respect to voltage applied to the embedded anisotropic strain actuator, a state-space representation is required after the steady-state solution is obtained. By perturbing Eqs. (3) and (4) using Eq. (5) about the calculated steady state, one gets

$$\begin{bmatrix} \frac{\partial F_S}{\partial X} - \frac{\partial F_L}{\partial X} & -\frac{\partial F_L}{\partial Y} \\ -\frac{\partial F_P}{\partial X} & \frac{\partial F_I}{\partial Y} - \frac{\partial F_P}{\partial Y} \end{bmatrix}_{\substack{X=\bar{X} \\ Y=\bar{Y}}} \begin{Bmatrix} \breve{X} \\ \breve{Y} \end{Bmatrix} +$$

$$\begin{bmatrix} \frac{\partial F_S}{\partial \dot{X}} - \frac{\partial F_L}{\partial \dot{X}} & 0 \\ 0 & \frac{\partial F_I}{\partial \dot{Y}} \end{bmatrix}_{\substack{X=\bar{X} \\ Y=\bar{Y}}} \begin{Bmatrix} \dot{\breve{X}} \\ \dot{\breve{Y}} \end{Bmatrix} + \tag{7}$$

$$\begin{bmatrix} \frac{\partial F_S}{\partial V} & 0 \\ 0 & 0 \end{bmatrix}_{\substack{X=\bar{X} \\ Y=\bar{Y}}} \{V\} = \begin{Bmatrix} 0 \\ 0 \end{Bmatrix}$$

from which the transient solution can be found. Since the aerodynamics is expressed as coupled through the blades, the system equations must be transformed to multi-blade coordinates resulting in a form of multi-harmonic series. In the present hover analysis, only the collective components of those need to be considered.

Eq. (7) is a state-space representation, and can be written in the following general form:

$$\begin{cases} \mathbf{E}X = \mathbf{A}\dot{X} + \mathbf{B}V \\ y = \mathbf{C}X + \mathbf{D}V \end{cases} \tag{8}$$

where y is the output vector of sensors embedded along the blade (strain gauge bridges configured for torsion or bending strain measurements). Frequency response function of the blade can be calculated using the following Laplace transform:

Note that the coefficient matrix **E** is usually singular due to the mixed formulation of the beam model.

$$\frac{\bar{y}(s)}{\bar{V}(s)} = \mathbf{C}(\mathbf{E}s - \mathbf{A})^{-1}\mathbf{B} + \mathbf{D} \tag{9}$$

3 ATR Blade Design

Aeroelastic design of the active twist blade was accomplished within the framework described above. The basic requirements for the ATR prototype blade come from an existing passive blade used by NASA Langley. The baseline (passive) system has been well studied and characterized along the years, and is representative of a typical production helicopter.[23] The new ATR blade is designed based on the external dimensions and aerodynamic properties of the existing baseline blade. Table 1 summarizes the general dimension and shape characteristics, and Table 2 presents the main structural characteristics of the baseline blade, as well as the result characteristics of the ATR prototype blade design. Finally, regarding actuation properties, the target was to provide an actuation level of approximately ±2° at the tip. This level of actuation authority is sufficient to experimentally investigate a wide range of IBC active twist applications.[23]

Different design studies including different cross-sectional actuation concepts were conducted to maximize actuation performance while satisfying stiffness, strength, and manufacturability constraints. A detailed investigation of the implications of distributing the torsional stiffness at different cross section members and the importance of having a multi-cell active cross-section analysis capability is presented in Ref. 21.

Table 1. General properties of the existing baseline rotor blade

Rotor type	Fully articulated
Number of blades, b	4
Blade chord, c	10.77 cm
Blade radius, R	1.4 m
Solidity, bc/pR	0.0982
Lock number	4.55
Airfoil shape	NACA 0012
Blade pretwist	–10° (linear from 0R to tip)
Hinge offset	7.62 cm
Root cutout	31.75 cm
Pitch axis	25% chord
Elastic axis	25% chord
Center of gravity	25% chord
Operational speed	687.5 rpm
Rotor overspeed	756 rpm

The chosen concept and converged structural design of the prototype Active Twist Rotor model blade is shown in Figs. 2 and 3. The final concept employs a total of 24 independent AFC actuators placed on the front spar only, and distributed in 6 stations along the radius. Even though it is not the highest actuation authority concept, the chosen one satisfies all the requirements and provides a lower cost option (where most of the cost comes from the AFC packs). The AFC laminae are embedded in the blade structure at alternating ±45° orientation angles that maximize the twist actuation capabilities of the active plies. With an even number of AFC plies, it is also possible to keep the passive structure of the rotor blade virtually elastically uncoupled. This allows independent actuation of blade torsional motion with practically no bending or axial actuation.

Structural integrity of the new blade design was evaluated based on the worst loading conditions, which are expected to occur within the rotor system operating envelope. In this design, forward flight with the maximum speed is selected as the loading criterion and CAMRAD II was used for the loads evaluation.

Table 2. Main characteristics of the ATR final design and the passive baseline blades

	Final Design	Requirement (Baseline)	% Difference
Mass per unit span (kg/m)	0.6960	0.6959	+0.01
x_{CG}/c	24.9 %	25%	–0.4
x_{TA}/c	30.8 %	25%	+23.2
K_{11} (axial) (N)	$1.637\ 10^{6}$	$2.0\ 10^{6}$	–18.2
K_{22} (torsional) (N-m^2)	$3.622\ 10^{1}$	$4.8468\ 10^{1}$	–25.3
K_{33} (flap bending) (N-m^2)	$4.023\ 10^{1}$	$4.3306\ 10^{1}$	–7.1
K_{44} (lead-lag) (N-m^2)	$1.094\ 10^{3}$	$7.0264\ 10^{3}$	–84.4
Lock No.	4.55	4.55	0.0
Section torsional inertia (kg-m^2/m)	$3.307\ 10^{-4}$	$3.1739\ 10^{-4}$	+4.2
1st torsion frequency @ 687.5 rpm	7.38/rev	7.37/rev	+0.1
Twist actuation @ 0 RPM (peak-to-peak, °/m)	4.52°	4°	+13.0
Maximum strain at the worst loading condition (@AFC) (μstrain)			
(1) Fiber direction	2,730		
(2) Transverse direction	2,730		
(3) Shear direction	5,170		

Then, the largest magnitudes of the aerodynamic loads are extracted and combined with the centrifugal loads in order to give the worst loading values and a safety factor of 1.5 is used. The developed design tool is used to convert the 1-D global beam loading into the stress/strain existing in constituent composite plies within the skin lay-up. By adopting maximum strain as the static failure criterion, the structural strength is confirmed.

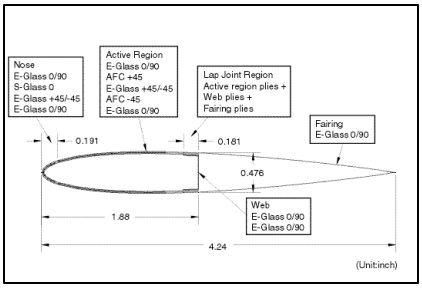

Figure 2. Schematic diagram of the final ATR blade section design. Dimensions are in inches.

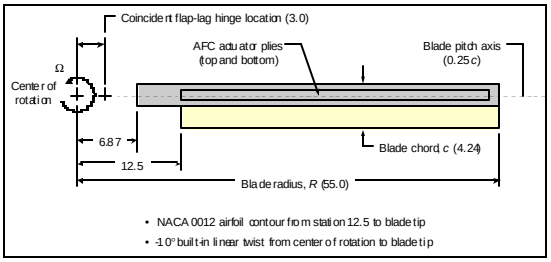

Figure 3. ATR aeroelastically scaled model blade geometry. Dimensions are in inches.

4 ATR Blade Prototype Manufacturing

The prototype blade was manufactured according to the final design described above. The aluminum blade mold used for the original baseline blade manufacturing was used again for this prototype. Also, besides the details described above, there were some additional needs on different miscellaneous elements.

4.1 Miscellaneous Items

Among the different elements that needed special attention during this phase, one of special importance is the blade root, which was totally modified from the original metal block attachment of the baseline blade. The concept adopted for this blade uses an integral graphite/epoxy construction in the exact external airfoil shape, with a small Rohacell foam core to provide the back pressure during cure. A total of 80 plies of IM7 unidirectional graphite/epoxy were cut and laid-up to form the $[0°, +45°, -45°, 90°]_{10}$ symmetric laminate about the foam core. This was chosen in order to provide enough strength for tensile, bending and torsional loads. Also, for continuity of the outboard lay-up, the root is wrapped around by the continuum skin EGlass plies of the outboard constant cross-section. Finally, three bolts in tandem do the mounting of the blade root with the hub attachment. The corresponding holes that go through the root block

are drilled using a diamond drill bit after the root stack is cured.

Regarding the AFC packs used for this prototype blade, similar design and manufacturing procedures adopted for the integral actuated blade[17] were used. The new blade geometry, however, required new pack dimensions and minor modifications on the gap between the AFC packs and the location of the solder flaps. The final geometry of the AFC packs is presented in Fig. 4. The manufacturing of all 24 individual AFC packs were performed by Continuum Control Corp., Burlington, Massachusetts, according to the specifications. Before using the packs on the composite construction, each of them were individually tested and their actuation and capacitance characterized at two different cycles: 3,000 V_{pp}/600 V_{DC} ("representative cycle") and 4,000 V_{pp}/1,200 V_{DC} ("extended cycle") for 1 and 10 Hz. The average free strain for the extended cycle was 1278 μstrain with a standard deviation of 228 μstrain.

To get the high voltage into the packs, a flexible circuit is inserted in the blade assembly and runs along the blade web. A total of six plies of such circuits were designed, each of which has 8 copper leads inside a kapton insulation. All Flex Inc., Northfield, Minnesota manufactured the flexible circuits according to the specifications. They were successfully tested for high voltage isolation prior to the blade construction. Once the flex circuits are in place, their square-colder pads are soldered to the flaps (connectors) on the AFC packs, and each individual circuit layer is attached together and to the web using film adhesive cured at 250°F.

Finally, the fabrication of the Rohacell foam core inserts and the tantalum ballast weights for the leading edge and web. The Rohacell foam blocks were machined at NASA Langley's Advanced Machining Development Laboratory to the desired airfoil section, with an extra 10~15 mil oversize to ensure the right back compression of the laminate against the mold walls during cure. The foam blocks for the fairing were hand cut and sanded using a metal guide tool. The ballast weights were also fabricated at NASA Langley. The leading edge weights were machined to the desired shape, and the web ones were cut as small plate-like pieces.

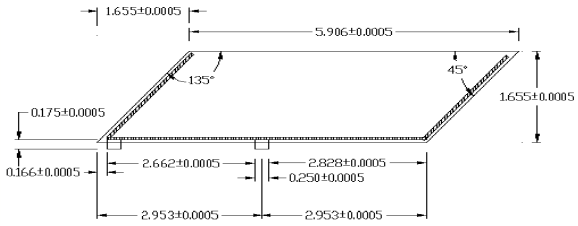

Figure 4. Final AFC pack design used in the ATR prototype blade

4.2 Testing Articles

Two testing articles were constructed prior to the final active prototype blade: a 1/3-span blade spar and a half-span blade spar (no-working AFC packs were used). Both were built with an aluminum attachment at the tip for gripping at the tensile testing machine. The first one was used primarily to debug the manufacturing process, including mold handling and usage, autoclave curing cycle (250°F, 90 min.—85 psi pressure was also used to support final closing of the mold), sliding of AFC packs in the prepreg laminate, the survivability of the AFC contact flaps through the curing cycle, the root construction, the Rohacell foam sizing and placement, and the attachment of strain gages on those foam pieces. The second testing blade was used primarily for testing the root strength and implementing modifications needed to the process identified from the first attempt. The improved manufacturing technique details used on the second blade checked all the steps to be followed on the full active blade.

After the tensile test, the second spar assembly was sliced to see any delamination of the plies or any voids trapped inside the assembly near the strain gages, and none was found. Also the weight of the spars was measured and compared with the target weight per unit length. Similarly, experiments were conducted to assess the spar torsional stiffness. Finally the fairing assembly of the same span length was attached and cured to the second spar successfully.

4.3 Prototype Blade

After the whole manufacturing process being well established, the fabrication of the ATR prototype blade followed. Before starting the wrapping of the prepreg plies around the foam, sensors need to be properly installed and tested. A total of 10 sets of full-bridge strain gauge sensors were embedded into the foam core surface and the wires ran through the small trough along the web. The 10 bridges were divided in six torsional strain gauges, three flap-bending strain gauges, all located at different spanwise stations, and one chordwise-bending strain gauge near the blade root. These strain gauges are used to monitor the deformation and load level during spinning on the hover stand or in the wind tunnel. They are also helpful for investigate individual pack actuation during bench tests.

The manufacturing of the spar assembly is conducted next. Two types of tantalum weight pieces are aligned and attached at the nose and rear web to give the desirable chordwise CG location and weight distribution. At the blade root, the stack of 80 graphite plies is inserted and at the discrete gap between the AFC packs and the root region is filled with SGlass

plies. The spar assembly is put inside the blade mold and sealed so vacuum can be built in the mold when inside the autoclave.

Once the spar is cured, the six flex circuit layers are soldered to the corresponding AFC flap connectors using high-temperature solder. They are then bonded to each other and to the web using strips of film adhesive. The final ATR prototype article can be seen in Fig. 5.

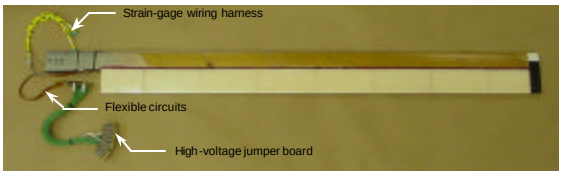

Figure 5. Final ATR prototype blade.

5 ATR Prototype Results

In what follows, different characterization tests were performed on the ATR prototype blade in order to validate the design and manufacturing procedures, and to verify the performance of the prototype article. Also numerical results obtained from the current theoretical model are presented for comparison at each stage of the experiments since the model was developed and expanded to enable variety of analyses, such as static actuation performance, frequency response at bench top, and aeroelastic response in hover condition.

5.1 Blade Torsional Stiffness Test

Since the blade torsional stiffness is an important parameter associated with the actuation authority of the blade, special attention is given to it. Tests were performed on the prototype blade before and after the fairing is attached. The tests were conducted on a specially built rig that applied a controlled couple at the tip of the blade, which stands vertically and is clamped at the root. A pair of laser sensors (Keyence LB-12, 2 μm resolution, 30~50 mm effective distance) was used to extract the rotation of a given station of the blade. A summary of the results in presented in Fig. 6, where the predicted results based on the developed thin-walled cross-sectional analysis and the more generic finite-element based VABS[26] are presented. As one can see, there is a significant increase (over 17%) on the blade torsional stiffness with the addition of the fairing. The overall correlation is considerably good considering that the experimental data has a spread of approximately ±2 N-m^2 for the spar measurements and ±4 N-m^2 for the complete blade. The thin-walled approximation consistently under-predicts the torsional stiffness by 20%. Some of that is due to the model not accounting for the foam core, ballast weights, and the presence of the flexible circuit. A more detailed asymptotical modeling (VABS) based on a finite element discretization of the warping field, and only including the effects of the foam core, shows a very good correlation with the experimental data.

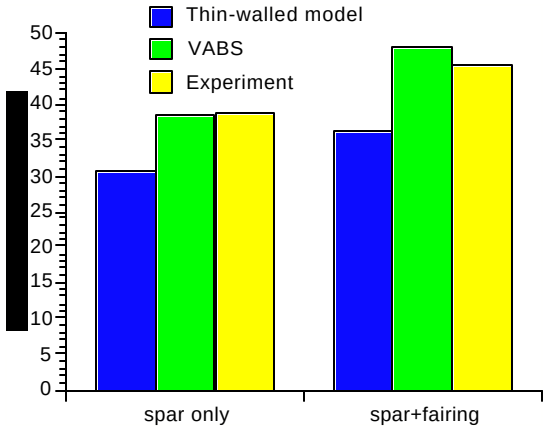

Figure 6. Torsional stiffness results for the spar and full blade–comparison between experimental and theoretical results

5.2 Bench Actuation Test

With the prototype blade cantilevered on the same rig as used for the stiffness tests, high voltage was applied to the packs and a pair of laser displacement sensors (LDS) was used to measure the rotation angle at the tip of the blade. The amplifier used in these tests was a TREK 663A, ±10 kV, 20 mA, 40 kHz limiting current and frequency, respectively.

5.2.1 Quasi-static actuation

Preliminary tests were performed on the spar first, and then on the whole assembly (spar + fairing) at very low excitation frequency (1 Hz). The tip twist angle measurements along with model predictions are presented in Table 4. Due to electric failures of the packs at higher voltages, tests were limited to a 2,000 V_{pp}/0 V_{DC} level. Based on the AFC material characterization conducted on this voltage level, the theoretical actuation prediction using the model developed in this study is carried out. As one can see, the present model overpredicts the low-frequency actuation by 20% to 27% considering the baseline LDS measurements. Notice, however, that the quasi-static cross-section actuation model has been validated well against other experimental data, and errors of no more than 15% were expected based on the available AFC material. Therefore, another set of measurements

was performed based on Projection Moiré Interferometry (PMI). The PMI is a noninvasive mean of remotely measuring shape, displacement, or deformation of an object. These measurements have an average accuracy of 0.056°±0.042° for the large scale system and 0.010°±0.012° for the small scale one for the blade rotation angle between 0° and 1° ("large" and "small scale system" are associated with the field of view, with the "large" one covering most of the blade's active region and the "small scale" being only about 30% span). Based on 18 working AFC actuators, the peak-to-peak tip twist at 2,000 V_{pp} is also included in Table 4 (last column). By correcting the twist actuation to account for the difference in the number of working AFCs, the experimental result from the PMI test is about 15% higher than the original LDS measurements, and the difference to the theoretical model is within 12%. This difference was somehow expected, among other things, due to the variation of AFC material properties (both active and passive properties).

Table 4. Peak-to-peak tip twist actuation of the ATR prototype blade (2,000 V_{pp}/0 V_{DC}, 1 Hz)

	Present Model	Experiment (LDS)	Exp. (PMI)
Spar only	1.4°	1.1°	-
Spar+fairing	1.2°	1.0°	1.1°*

* only 18 active AFC packs.

5.2.2 Non-rotating frequency response

The non-rotating dynamic characteristics of the blade can be evaluated from the frequency response of an applied sinusoidal excitation to the AFC actuators. Figs. 7 and 8 show sample of the results of the strain gauges embedded in the blade and the LDS (for tip twist angle) readings and the theoretical predictions of the present model at several blade stations as function of the AFC actuation.

As one can see, the first torsional mode is clearly identified at approximately 85 Hz, and this result matches well with model prediction. The peaks at the torsional natural frequency in the model prediction are found quite higher (tend to infinite) than those in the bench test results since no damping is included in the structural model. This already indicates that some structural damping should be added to the model. Once the aerodynamics is included in the problem, its damping will bring the peak to finite amplitude. While the strain results could be obtained at high excitation voltages, the dynamic tip twist was measured at low voltages due to the limitation on the range of the laser sensors. At 400 V_{pp}, the peak-to-peak tip twist response of the blade is approximately 3.5°. Such an increased dynamic response around the first torsional natural frequency is expected to affect the twist response over the frequency range of interest when the blade is rotating. It makes the frequency response quite flat after 1P (11.5 Hz), compensating for the inherent degradation authority of the piezoelectric material with frequency. Therefore, the theoretical model presented herewith shows very good correlation with experimental test on the frequency response for both tip twist actuation and torsional deformation of the active blade.

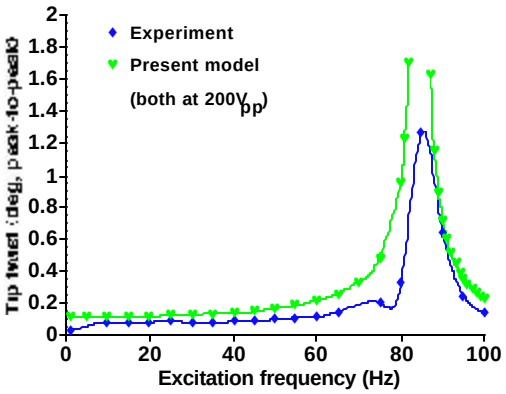

Figure 7. Tip twist response of the ATR prototype blade on the bench

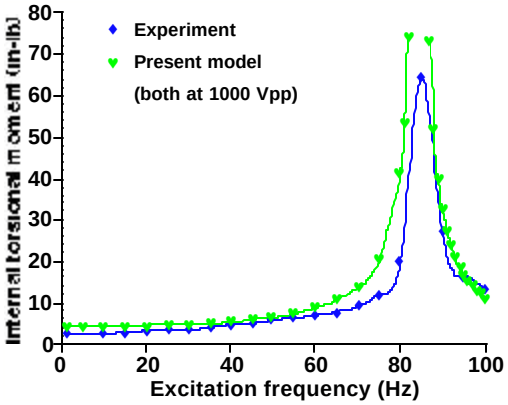

Figure 8. Torsional moment at 31% blade radius of the ATR prototype blade on the bench

5.3 Hover Test

The ATR prototype blade was used with three other similar passive blades for hover testing as a four-bladed fully-articulated rotor system inside the NASA Langley TDT (shown in Fig. 1). The test conditions include harmonic sine dwell actuation in either normal air or heavy gas medium environment. The rotational speed was varied (full 688 rpm and 10% below that), as well as the collective pitch setting (0°, 4° and 8°).

The blade tracking and balance was successfully accomplished by adjusting the active blade weight and its pitch angle. In order to provide high voltage to the rotating active blade, a specially designed high-voltage slip ring was installed between the fixed system and the rotating one. During the hover tests, a total of 26 data channels were monitored and stored to investigate the aeroelastic characteristics of both the overall rotor system and the individual blade. These signals include 6-component rotor system balance loads, strain gauges embedded in the active blade, pitch link loads, etc.

The acquired signal data in time is then processed to obtain the transmissibility of the system with respect to the sinusoidal actuation of the active blade in frequency-domain. The undesirable signal noise is filtered from the data by adopting a simple smoothing algorithm. The transfer function can be obtained by the output signal divided by input signal, both of which are transformed to frequency-domain by a fast-Fourier transform (FFT) technique. Since sine dwell was used in the test, one set of data corresponding to each discrete frequency generates one point in the transfer function plots.

From the theoretical model developed in this study, the frequency response of the ATR prototype blade can be computed for the hover condition. As sample results, Fig. 9 shows the internal torsional moment at 31% blade radial station and its comparison with the experimental data for the case of heavy gas environment, 688 rpm, 2,000 V_{pp} excitation, and varying collective pitch settings (0°, 4°, 8°). As one can see from both magnitude and phase of the torsion gage readings, the actuation authority is insensitive to the blade static loading (represented by the different collective settings). Also, the first torsion resonance frequency appears at about 70 Hz (6.3 P), lower than the bench result (85 Hz), which is associated with the pitch link flexibility, the aerodynamic damping effects, and the effective change on the total length of the blade (due to its mounting on the hub). Even though the analytical model overpredicts magnitude of the blade deformation in the low frequency actuation regime, the correlation is fairly good. Moreover, the analytical prediction clearly confirms the previous experimental findings that the actuation authority is insensitive to the blade static loading.

The frequency response function of the internal torsional moment at 31% span location for varying test medium density is shown in Fig 10. As can be seen, the medium density variation does not influence the actuation authority, except at the torsional resonance frequency due to the change in the aerodynamic damping with density. It is also found that the theoretical results follow well the experimental trends so that the peak magnitude around the torsional resonant frequency increases as the test medium density decreases. However, quantitatively the model still overpredicts the experimental data.

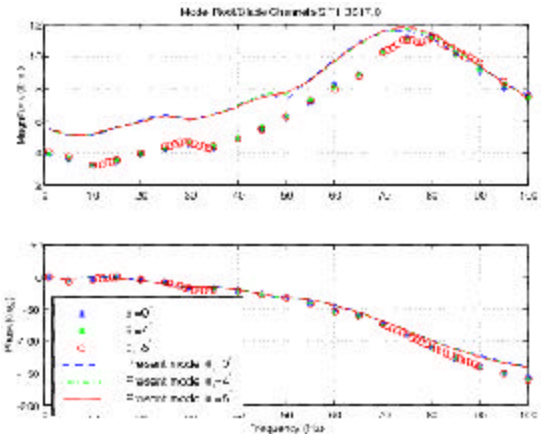

Figure 9. Torsional moment at 31% blade radius of the ATR prototype blade in hover (688 rpm, heavy gas, 0.00472 slug/ft^3 density, 2.000 V_{pp} actuation)

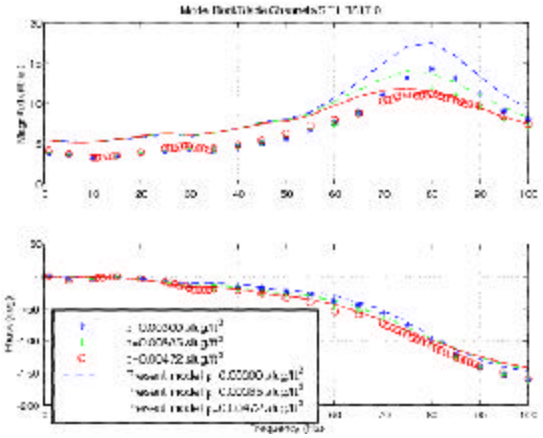

Figure 10. Torsional moment at 31% blade radius of the ATR prototype blade in hover (688 rpm, 2,000 V_{pp} actuation, θ_o = 8°, variable medium density).

Frequency response sensitivity with respect to rotor rotational speed is shown in Fig. 11 for 688 (100%) and 619 (90%) rpm. Again, the actuation is quite insensitive to perturbation from the centrifugal loads away from the torsion resonant peak. Around that point, the variation of the aerodynamic damping is responsible for the changing in magnitude of the internal torsional moment. The theoretical model predicts those trends very well, and again overpredicts the magnitude of the torsional moment.

Overall, the trends are excellent. The degradation of the actuation performance with frequency is well captured and can be observed at low frequency range (below 10 Hz) on all the hover results. The structural resonance, even though occurring at higher frequency, has a broad bandwidth that influences over the low frequency range, bringing the twist actuation up. The phase correlation is excellent, both qualitatively as

well as quantitatively. The magnitude of the vibratory torsional moment has been consistently overpredicted. The relative error goes from less than 1% to over 50% (in few particular spots). The lack of structural damping is the primary source responsible for such discrepancies around the peaks as already concluded from the bench results. However, that alone does not explain the discrepancies at low excitation frequencies. Another source of damping present in the experiment and not taken into account in the present model is a lead-lag damper present in the experimental setup. The coupled pitch-flap-lag motion may bring some of those effects to influence the results above.

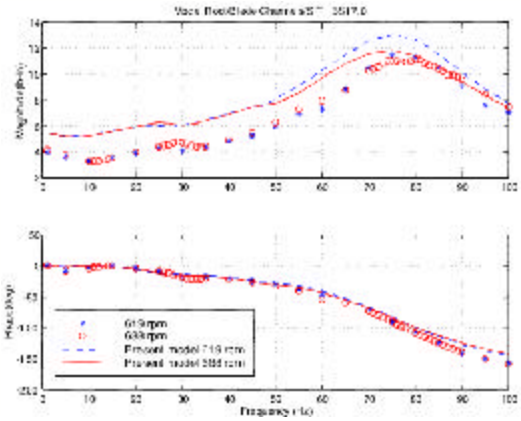

Figure 11. Torsional moment at 31% blade radius of the ATR prototype blade in hover (2,000 V_{pp} actuation, $\theta_o = 8°$, .00472 slug/ft^3 density).

To estimate the potential capability of vibration reduction using the current ATR blade concept, CAMRAD II[20] is used in forward flight conditions. Its model employs an equivalent torque couple to represent the twist actuation generated by the actuators. The present cross-sectional analysis provides the active moment to be used in that analysis. Once the CAMRAD II model is calibrated, similar correlation with the present model for this experimental data can be verified.[23] Fig. 12 shows the 4P vertical hub shear force that the ATR system is predicted to be subjected at a given forward flight condition as function of the phase of the applied actuation. Without actuation, the projected 4P vertical force is approximately 6 lb. The four-active bladed system under 2,000 V_{pp} actuation (equivalent to an actuation ratio of 0.5 in Fig. 12) is expected to reduce the 4P vibration of about 60% to 80% at μ=0.30, C_T/σ=0.075 and C_x/σ=-0.0046.

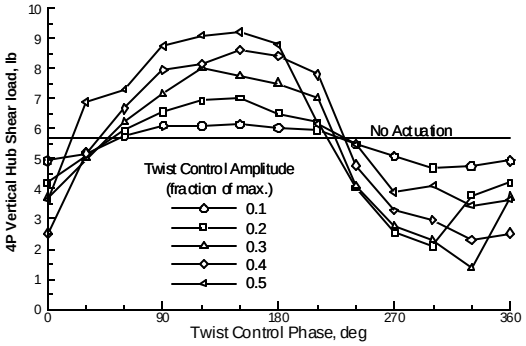

Figure 12. Variation of thrust induced by twist actuation at ATR system in forward flight (μ=0.30, C_T/σ=0.075, C_D/σ=-0.0046).

6 Concluding Remarks

This paper presented the design framework, manufacturing, and bench and hover test results for an active rotor blade concept. The active rotor blade is designed to reduce rotor vibratory loads by piezoelectrically controlled twisting on the individual blades.

Experimental structural characteristics of the prototype blade compare well with design goals, and modeling predictions correlate fairly with experimental results. Preliminary bench actuation tests show lower twist performance than originally expected, and are due to electric failure of some of the actuators at high electric fields. A study of the frequency response of an active blade was conducted for both non-rotating and hover conditions. Correlation between the developed model and the ATR experimental data was very good. Both analytical and experimental results show that the twist actuation authority of the ATR blade is independent of the collective setting up to approximately 10P, and the only dependence on rpm and altitude show near the torsional resonance frequency due to its dependency on the aerodynamic damping. For all the aeroelastic results, the phase correlation of the vibratory twist moment was excellent. The model, however, generally overpredicts the magnitude of the moment. The overprediction around the resonance frequency was expected due to the lack of structural damping. The discrepancies at low frequency are between 1% and 50% (in few frequency locations) which are associated with uncertainties on the active material properties, hub dynamic properties, and the unmodeled led-lag damper. Future tests and simulations will be extended to forward flight condition for a full validation of the concept. Finally, based on a calibrated model, estimation of 4P vertical hub shear force at μ=0.30 shows potential for 60% to 80% vibratory load reduction. The presented modeling, design, manufacturing, and bench and hover test results on this prototype blade set the foundation for future

development of the ATR concept for IBC in forward flight. This will be presented in a future paper.

7 Acknowledgement

This work is sponsored by NASA Langley Research Center under the cooperative agreement NCC 1-323.

8 References

1. Loewy, R. G., "Recent Developments in Smart Structures with Aeronautical Applications," Proceedings of the 37th Israel Annual Conference on Aerospace Sciences, February 26–27, 1997.
2. Friedmann, P. P., "The Promise of Adaptive Materials for Alleviating Aeroelastic Problems and Some Concerns," Proceedings of Innovation in Rotorcraft Technology, Royal Aeronautical Society, London, United Kingdom, June 24–25, 1997.
3. Spangler, R. L., Jr. and Hall, S. R., "Piezoelectric Actuators for Helicopter Rotor Control," Proceedings of the 31st AIAA/ASME/ AHS Structures, Structural Dynamics, and Materials Conference, Apr. 2-4, 1990, Technical Papers, AIAA Paper No. 90-1076, 1990, pp. 1589-1599.
4. Prechtl, E. F. and Hall, S. R., "Design and Implementation of a Piezoelectric Servo-Flap Actuation System for Helicopter Rotor Individual Blade Control," AMSL Report #00-3, Active Materials and Structures Laboratory, Massachusetts Institute of Technology, January 2000.
5. Samak, D. and Chopra, I., "A Feasibility Study to Build a Smart Rotor: Trailing Edge Flap Actuation," SPIE Smart Structures and Materials Conference, Feb. 1-4 1993, Smart Structures and Intelligent Systems, Proceedings, Vol. 1917, Part 1, 1993, pp. 225-237.
6. Straub, F., "A Feasibility Study of Using Smart Materials for Rotor Control," Proceedings of the American Helicopter Society 49th Annual Forum, St. Louis, Missouri, May 1993.
7. Millot, T. and Friedmann, P., "Vibration Reduction in Helicopter Rotors Using an Actively Controlled Partial Span Trailing Edge Flap Located on the Blade," NASA Contractor Report 4611, June 1994.
8. Giurgiutiu, V., "Recent Advances in Smart-Material Rotor Control Actuation," Proceeding of the 41st AIAA/ASME/ASCE/AHS/ASC Structures, Structural Dynamics, and Materials Conference -Adaptive Structures Forum, Atlanta, Georgia, April 4-6, 2000, AIAA Paper No. 2000-1709.
9. Fulton, M. V. and Ormiston, R., "Hover Testing of a Small-Scale Rotor with On-Blade Elevons," Proceedings of the American Helicopter Society 53rd Annual Forum, Virginia Beach, VA, April 29-May 1, 1997.
10. Barrett, R., "Intelligent Rotor Blade Structures Development Using Directionally Attached Piezoelectric Crystals," M.S. thesis, University of Maryland, College Park, MD, 1990.
11. Chen, P. and Chopra, I., "Hover Testing of Smart Rotor with Induced-Strain Actuation of Blade Twist," AIAA Journal, Vol. 35, No. 1, 1997, pp. 6–16.
12. Wilkie, W. K., Park., K. C., and Belvin, W. K., "Helicopter Dynamic Stall Suppression Using Active Fiber Composite Rotor Blades," AIAA Paper No. 98-2002, Proceedings of the 39th AIAA/ASME/AHS Structures, Structural Dynamics, and Materials Conference, Long Beach, California, April 20–23, 1998.
13. Rodgers, J. P. and Hagood, N. W., "Development of an Integral Twist-Actuated Rotor Blade for Individual Blade Control," AMSL Report #98-6, Active Materials and Structures Laboratory, Massachusetts Institute of Technology, October 1998.
14. Bent, A., Hagood, N., and Rodgers, J., "Anisotropic Actuation with Piezoelectric Fiber Composites," Journal of Intelligent Material Systems and Structures, Vol. 6, May 1995, pp. 338–349.
15. Cesnik, C. E. S. and Shin, S. J., "On the Modeling of Active Helicopter Blades," International Journal of Solids and Structures, in press, 2000.
16. Hodges, D. H., "A Mixed Variational Formulation Based on Exact Intrinsic Equations for Dynamics of Moving Beams," International Journal of Solids and Structures, Vol. 26, No. 11, 1990, pp. 1253–1273.
17. Shang, X. and Hodges, D. H., "Aeroelastic Stability of Composite Rotor Blades in Hover," Proceedings of the 36th AIAA/ASME/AHS Structures, Structural Dynamics, and Materials Conference, New Orleans, Louisiana, April 10–12, 1995.
18. Shin, S. J. and Cesnik, C. E. S., "Dynamic Response of Active Twist Rotor Blades," Proceeding of the 41st AIAA/ASME/ASCE/ AHS/ASC Structures, Structural Dynamics, and Materials Conference -Adaptive Structures Forum, Atlanta, Georgia, April 4-6, 2000, AIAA Paper No. 2000-1711.
19. Peters, D. A. and He, C. J., "A Closed Form Unsteady Aerodynamic Theory for Lifting Rotor in Hover and Forward Flight," Proceedings of the American Helicopter Society 43rd Annual Forum, St. Louis, Missouri, May, 1989.
20. Wilkie, W. K., Wilbur, M. L., Mirick, P. H., Cesnik, C. E. S., and Shin, S.-J., "Aeroelastic Analysis of the NASA/ARMY/MIT Active Twist Rotor," Proceedings of the American Helicopter Society 55th Annual Forum, Montréal, Canada., May 25–27, 1999.
21. Cesnik, C. E. S. and Shin, S. J., "On the Twist Performance of a Multiple-Cell Active Helicopter Blade," Journal of Smart Materials and Structures-Special Edition for Rotorcraft, accepted, 2000.
22. Cesnik, C. E. S. and Hodges, D. H., "VABS: A New Concept for Composite Rotor Blade Cross-Sectional Modeling," Journal of the American Helicopter Society, Vol. 42, No. 1, 1997, pp. 27–38.
23. Wilbur, M. L., Yeager Jr., W. T., Wilkie, W. K., Cesnik, C. E. S., and Shin, S. J., "Hover Testing of the NASA/Army/MIT Active Twist Rotor Prototype Blade," American Helicopter Society 56th Annual Forum, Virginia Beach, Virginia, May 2—4, 2000.